JOURNAL OF VIROLOGY, Feb. 2010, p. 1828–1837 Vol. 84, No. 4
0022-538X/10/$12.00 doi:10.1128/JVI.01890-09

Estimation of the Size of Genetic Bottlenecks in Cell-to-Cell Movement of *Soil-Borne Wheat Mosaic Virus* and the Possible Role of the Bottlenecks in Speeding Up Selection of Variations in *trans*-Acting Genes or Elements[▽]§

Shuhei Miyashita[1,2,3]* and Hirohisa Kishino[1]

Graduate School of Agricultural and Life Sciences[1] and Asian Natural Environmental Science Center (ANESC),[2] University of Tokyo, 1-1-1 Yayoi, Bunkyo-ku, Tokyo 113-8657, Japan, and PRESTO, Japan Science and Technology Agency (JST), 4-1-8 Honcho Kawaguchi, Saitama 332-0012, Japan[3]

Received 6 September 2009/Accepted 20 November 2009

Genetic bottlenecks facilitate the fixation and extinction of variants in populations, and viral populations are no exception to this theory. To examine the existence of genetic bottlenecks in cell-to-cell movement of plant RNA viruses, we prepared constructs for *Soil-borne wheat mosaic virus* RNA2 vectors carrying two different fluorescent proteins, yellow fluorescent protein (YFP) and cyan fluorescent protein (CFP). Coinoculation of host plant leaves with the two RNA2 vectors and the wild-type RNA1 showed separation of the two vector RNA2s, mostly within seven to nine cell-to-cell movements from individual initially coinfected cells. Our statistical analysis showed that the number of viral RNA genomes establishing infection in adjacent cells after the first cell-to-cell movement from an initially infected cell was 5.97 ± 0.22 on average and 5.02 ± 0.29 after the second cell-to-cell movement. These results indicate that plant RNA viruses may generally face narrow genetic bottlenecks in every cell-to-cell movement. Furthermore, our model suggests that, rather than suffering from fitness losses caused by the bottlenecks, the plant RNA viruses are utilizing the repeated genetic bottlenecks as an essential element of rapid selection of their adaptive variants in *trans*-acting genes or elements to respond to host shifting and changes in the growth conditions of the hosts.

Plant RNA viruses change their genomes so rapidly that variant viruses with altered biological properties are often found after prolonged growth of infected plants or after serial mechanical inoculations (26, 33). Furthermore, inoculation of less-fit artificial mutants produces revertants or pseudo-revertants even after short infection times (12, 14). The rapid evolution of plant RNA viral genomes is achieved not only by high mutation rates due to error-prone replication by the nonproofreading viral RNA-dependent RNA polymerase (19) but also by rapid selection and strong genetic drift. Generally, narrow genetic bottlenecks facilitate the fixation and extinction of variants in populations (15), and viral populations are no exception to this theory.

Plant RNA viruses are known to face many narrow genetic bottlenecks during their life cycles (23). The life cycles of most plant RNA viruses are as follows: After replicating in cells, viruses move from cell to cell through plasmodesmata, which connect the cytoplasms of adjacent cells separated by cell walls in plant tissue. Following the establishment of infection in cells and cell-to-cell movements, the viruses expand their infected regions, spreading to the veins and moving through the vascular system and infecting the plant systemically. Some plant RNA viruses are transmitted through the seeds or via mechanical injuries, but most are transmitted from plant to plant by biological vectors such as insects, nematodes, and fungi. Previous studies have found that genetic bottlenecks occur during the transfer from lower leaves to upper leaves in systemic infections of *Wheat streak mosaic virus* (WSMV) (11), *Tobacco mosaic virus* (TMV) (24), and *Cucumber mosaic virus* (CMV) (18) and during the transfer from one tiller to another tiller of WSMV (11). Vector transmissions were also shown to act as genetic bottlenecks for WSMV (11), CMV (1, 3), and *Potato virus Y* (PVY) (20). With the exception of PVY, the typical method for detecting genetic bottlenecks has been to observe the spatial separation of closely related strains or artificial synonymous mutants inoculated as mixed populations: the narrower the genetic bottleneck, the more frequently the spatial separation should be observed. Using this idea with mathematical analyses, WSMV was estimated to infect a new tiller starting with four genomes (9), TMV was estimated to infect the upper leaves starting with 10 genomes (24), and CMV was estimated to infect a new plant starting with one to two particles after aphid transmission (3). Studies of PVY using sets of host plant cultivars with or without resistance genes and mixed strains of viruses with or without resistance-breaking abilities also estimated the number of virus particles transmitted by an aphid vector to be 0.5 to 3.2 on average (20).

However, genetic bottlenecks in cell-to-cell movement of viruses have not been well characterized, although these occurrences are likely (11) and have been expected to be important for understanding the life cycle and population dynamics of plant RNA viruses. The size of genetic bottlenecks in cell-to-cell movement can be referred to as "multiplicity of infec-

* Corresponding author. Mailing address: Asian Natural Environmental Science Center (ANESC), University of Tokyo, 1-1-1 Yayoi, Bunkyo-ku, Tokyo 113-8657, Japan. Phone and fax: 81-3-5841-8036. E-mail: smiyashita@live.jp.

§ Supplemental material for this article may be found at http://jvi.asm.org/.

▽ Published ahead of print on 2 December 2009.

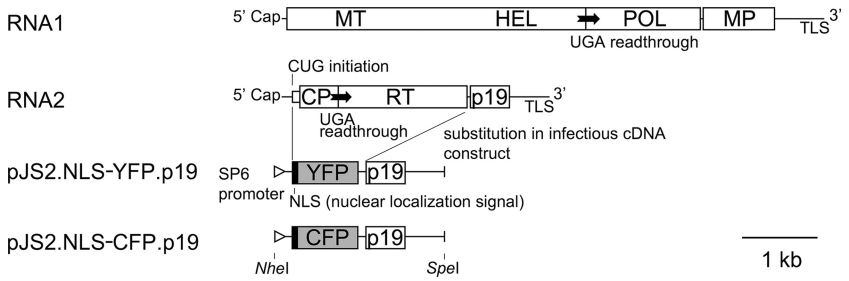

FIG. 1. Genome structure of SBWMV and cDNA constructs for fluorescent protein vector RNA2s used in this study. ORFs are indicated by rectangles. MT, methyltransferase domain of replicase; HEL, helicase domain of replicase; POL, RNA polymerase domain of replicase; MP, cell-to-cell movement protein; TLS, tRNA-like structure; CP, capsid protein; RT, readthrough region translated by readthrough of UGA stop codon for CP; p19, 19-kDa protein with RNA silencing suppressor activity.

tion (MOI) in plant tissue colonization," and only a recent study showing that the estimated MOI of TMV is between 6 and 1 to 2 (10) indicates the occurrence and the size of genetic bottlenecks in cell-to-cell movement of a plant RNA virus. In this paper, we also show the occurrence of narrow genetic bottlenecks during cell-to-cell movement of a plant RNA virus, *Soil-borne wheat mosaic virus* (SBWMV, type species of the genus *Furovirus*), by observing the spatial separation of RNA2 vectors carrying different fluorescent proteins, yellow fluorescent protein (YFP) and cyan fluorescent protein (CFP). Both of the fluorescent proteins were expressed as fusion proteins to the N-terminal nuclear localization signal (NLS) peptide from *Simian virus 40* (SV40) large T antigen, which enabled us to observe and count the infected cells accurately using nuclear fluorescence. Numerical data were analyzed to estimate the size of bottlenecks. We also carried out a simulation to show that, due to the narrow genetic bottlenecks, rapid selection occurs even on *trans*-acting elements in plant RNA virus genomes, overcoming the negative effect of complementation among adaptive and defective genomes in each intracellular population. We discuss the possible roles of the bottlenecks in the life cycle and evolution mechanisms of plant RNA viruses.

MATERIALS AND METHODS

Plants. Fully expanded leaves of *Chenopodium quinoa* were used for inoculation after growth at 22°C for 4 to 6 weeks after sowing. Wheat (cv. Fukuho) leaves were used for inoculation after growth at 17°C for 2 weeks after sowing. *C. quinoa* is a local lesion host of *Soil-borne wheat mosaic virus* (SBWMV) used in this study, and wheat is a natural systemic host of SBWMV.

Viral cDNA constructs. Infectious cDNA constructs for a Japanese Tochigi strain of SBWMV (SBWMV-JT), pJS1 for RNA1 and pJS2 for RNA2, were described by Yamamiya and Shirako (35). pJS2 was used as a parental vector construct for fluorescent protein gene expression. The N-CP-RT region was replaced with fluorescent protein gene sequences. YFP-coding cDNA was prepared by introducing variations in SYFP2 (17) into a SuperGlo GFP (sgGFP) gene sequence derived from pQBI25 (TaKaRa BIO, Japan). CFP-coding cDNA was prepared by introducing variations in SCFP3A (17) into the sgGFP gene sequence. The NLS coding sequence from *Simian virus 40* (SV40) large T antigen and the franking sequence (translated into MDKAELIPEPPKKKRKVEL; underlined sequence indicates NLS) were derived from the pGAD-c1 vector (13) and added upstream of each fluorescent protein coding sequence. The resulting cDNA constructs were named pJS2.NLS-YFP.p19 and pJS2.NLS-CFP.p19.

***In vitro* transcription and inoculation.** *In vitro* transcription of pJS1- and pJS2-derived constructs were done in the presence of a cap analog using SP6 RNA polymerase (TaKaRa BIO). For reverse transcriptase PCR (RT-PCR) analysis, template DNA was digested with DNase (Promega) prior to inoculation. Transcripts were quantified by a Qubit fluorometer (Invitrogen) and added to inoculation buffer (0.1 M NaCl, 0.1 M Tris-HCl pH 8.5) at the concentrations of 7.5 ng/μl of RNA1 and 5.0 ng/μl of RNA2s unless otherwise noted and were rubbed onto the surface of assay plant leaves using carborundum as an abrasive. Inoculated plants or leaves were rinsed with water and placed in the dark at 17°C.

Fluorescent light microscopy observations. YFP and CFP fluorescence was observed using a fluorescent light microscope (Olympus IX70 and IX-FLA, Japan) with NIBA and U-MCFPHQ filter sets (Olympus), respectively. The images were captured using a charge-coupled-device (CCD) camera (KEYENCE VB-7010, Japan). Photoshop Element Ver 4.0 (Adobe) was used for converting the color of CFP fluorescence images into magenta and merging with YFP fluorescence images.

Total RNA extraction, RT-PCR, and cloning. Total RNA was extracted using QuickGene 800 (FUJIFILM) after grinding of the frozen leaf samples by a Mixer Mill MM300 (Qiagen). SBWMV RNA2 in total RNA or RNA2 transcripts were amplified by a PrimeScript One Step RT-PCR kit (TaKaRa BIO) using two sets of primers: TP292 (5′-AACGTGCGACGTTGAGA-3′) and TP41 (5′-CTGCT GTGTAATAGCAG-3′) for amplifying almost the entire RNA2 transcript; TP292 and TP290 (5′-CACTGTGACGATACTTA-3′) for amplifying the YFP or CFP coding region (see Fig. 3A). DNA fragments amplified using TP292 and TP290 were cloned into a pGEM-T TA-cloning vector (Promega) for sequencing.

Nucleotide sequence accession numbers. The nucleotide sequences for pJS2.NLS-YFP.p19 and pJS2.NLS-CFP.p19 are available from the DNA Data Bank of Japan (DDBJ) (accession numbers AB499725 and AB499726, respectively).

RESULTS

Observation of spatial separation between SBWMV vectors carrying different fluorescent proteins. *Soil-borne wheat mosaic virus* (SBWMV), a positive-strand plant RNA virus, has a bipartite genome consisting of two RNA molecules, RNA1 and RNA2 (27, 28). RNA1 encodes replication proteins and a movement protein (MP) for cell-to-cell movement (2). RNA2 encodes the capsid protein (CP) and two CP-containing proteins: CP-RT, produced by readthrough of a stop codon, and N-CP, initiated from an upstream CUG codon (25). RNA2 also encodes a cysteine-rich protein, p19, with RNA silencing suppressor activity (29). As CP and the two CP-containing proteins are not required for replication or cell-to-cell movement (35; M. Miyanishi and Y. Shirako, unpublished data), we replaced their open reading frames (ORFs) in the infectious cDNA clone of RNA2 (pJS2) with YFP or CFP sequences fused to N-terminal NLS sequences to prepare virus vectors for YFP or CFP expression (Fig. 1). The YFP and CFP genes used in this study differ by 10 nucleotides, resulting in six differing amino acids. Transcripts from these cDNA clones, named RNA2.NLS-YFP.p19 and RNA2.NLS-CFP.p19, were mixed with the wild-type RNA1 transcripts and inoculated onto *Chenopodium quinoa* leaves. Leaves were placed in the dark at 17°C and observed under a fluorescent microscope at appro-

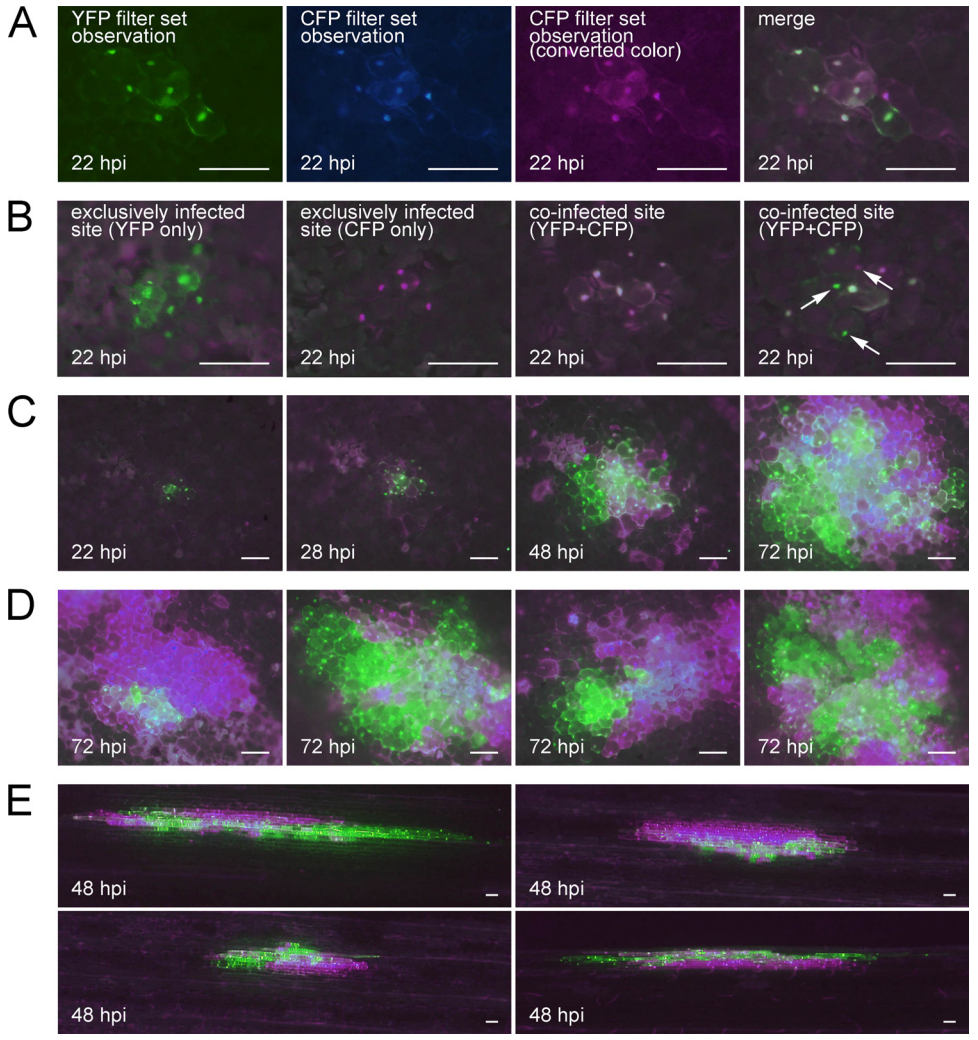

FIG. 2. Observation of the spatial separation between SBWMV vectors carrying different fluorescent proteins in local lesion host *C. quinoa* (rows A to D) and natural host wheat (row E) leaves. (A) An example of preparation of a merged image. The YFP image (first panel) and CFP image (second panel) were taken separately, and the CFP image was converted to magenta (third panel). Then, the YFP image and converted CFP image were merged (fourth panel). Rows B to D show merged images. (B) Infected sites at 22 hpi. The first and second panels show sites exclusively infected by the YFP vector and CFP vector, respectively. The third and fourth panels show coinfected sites, and the white arrows in the fourth panel indicate the cells showing exclusive infection by one of the two vectors. (C) Time course observation of a coinfected site at 22, 28, 48, and 72 hpi. (D) Coinfected sites at 72 hpi. (E) Coinfected sites in wheat at 48 hpi. All the bars represent 100 μm.

priate time points. YFP and CFP fluorescence images were taken separately and merged after the color of CFP fluorescence images was converted to magenta (an example of preparation of merged images is shown in Fig. 2A). YFP and CFP proteins were confirmed to mature at similar time points by inoculating barley protoplasts with the transcripts (data not shown). Inoculation without RNA1 or inoculation of template DNA did not show any fluorescence, indicating that fluorescent protein expression requires replication of RNA2 by an RNA1-encoded viral replicase (data not shown).

At 22 hours post inoculation (hpi), most of the infected sites already consisted of several infected cells. Although some of the infected sites showed only YFP or CFP fluorescence (Fig. 2B, first and second panels; Table 1), most of the infected sites showed both YFP and CFP fluorescence (Fig. 2B, third and fourth panels; Table 1), indicating that coinfection of initial cells with both the RNA2.NLS-YFP.p19 and RNA2.NLS-CFP.p19 vector viruses occurred frequently. Increasing the concentration of RNA transcripts used for inoculation did not change the number of infected sites or the frequency of coinfection (Table 2). This result indicates that the concentration of inoculated RNA was high enough to saturate all the possible infection sites. Within coinfected sites, most of the cells showed coinfection, but some of the cells showed exclusive infection by YFP or CFP vector virus (Fig. 2B; exclusively infected cells can be found in the fourth panel and are indicated by white arrows). This spatial separation between YFP and CFP vector viruses progressed corresponding to the expansion of the infected regions (Fig. 2C), and at 72 hpi, most of the infected sites showed absolute separation of the YFP and CFP vector in newly infected frontier cells by 7 to 9 cell-to-cell movements (Fig. 2D). The occurrence of spatial

TABLE 1. Number of infected sites and cells coinfected or exclusively infected by one of the virus vectors

Site/class of cells observed or calculated	Cells	Type of fluorescence observed		
		YFP only	YFP+CFP	CFP only
Infected sites at 22 hpi		14	179	10
Cell-0+Cell-1 (22 hpi)	Total no. of cells[a]	77	945	82
Cell-0+Cell-1+Cell-2 (28 hpi)		198	1163	232
Cell-0	No. (%) of cells per class[b]	0 (0.0%)	158 (100.0%)	0 (0.0%)
Cell-1		77 (8.1%)	787 (83.2%)	82 (8.7%)
Cell-2		140.2 (17.1%)	504.6 (61.6%)	174.2 (21.3%)

[a] Total number of cells with coinfection or exclusive infection in coinfected sites. Data for Cell-0+Cell-1 were collected from 158 sites with 5 to 9 infected cells at 22 hpi. Data for Cell-0+Cell-1+Cell-2 were collected from 86 coinfected sites with 10 to 30 infected cells at 28 hpi.
[b] Number and percentage of cells with coinfection or exclusive infection in coinfected sites. Numbers for Cell-1 and Cell-2 were obtained by simple calculation as described in the text.

separation was also observed when wheat leaves were used as a host (Fig. 2E).

Mutation frequency of the fluorescent protein genes. In order to check whether mutation causes loss of fluorescence in the above experiments, we carried out RT-PCR of RNA2 vectors. When total RNA samples extracted from *C. quinoa* leaves inoculated with RNA1 and RNA2.NLS-YFP.p19 at 28, 48, or 72 hpi were subjected to RT-PCR, neither the primer set for almost entire RNA2 vector (TP292 and TP41) nor that for fluorescent protein coding regions (TP292 and TP290) (Fig. 3A) detected a distinct amount of cDNA products shorter than the correct size (Fig. 3B), indicating that deletion mutation is not a frequent event. TA cloning and sequencing of the RT-PCR product of the 72-hpi total RNA sample using the latter primer set (TP292 and TP290) showed that, out of 23 clones, two clones had deletion mutations and eight clones had point mutations (i.e., nucleotide substitutions and single-nucleotide insertions) in the fluorescent protein coding region (Table 3). However, the frequency of point mutation was not higher than that found in the control experiments cloning the RT-PCR product of the inoculated RNA transcript or the PCR product of template DNA used for transcription (Table 3). These results indicated that the point mutations detected occurred mainly in the PCR process, but deletion mutations occurred during virus infection and caused loss of fluorescence, although the frequency of deletion mutations is less than 10% until 72 hpi. We also tested the possibility of recombination during infection, but no recombination between YFP and CFP vectors was observed in 21 clones sequenced after cloning of the RT-PCR products of total RNA samples isolated from coinoculated leaves collected at 72 hpi (data not shown).

TABLE 2. Number of infected sites and frequency of coinfection in decreased or increased concentrations of inoculated RNA transcripts[d]

Concn of transcripts (ng/μl)[e]	No. of infected sites per cm^2	Coinfection frequency (%)
3.75 + 1.25 + 1.25[a]	14 ± 3	75 ± 8
7.5 + 2.5 + 2.5[b]	30 ± 8	85 ± 5
15 + 5 + 5[c]	25 ± 8	86 ± 6

[a] Decreased (0.5×) concentration of the RNA transcripts.
[b] Usual (1×) concentration of the RNA transcripts.
[c] Increased (2×) concentration of the RNA transcripts.
[d] Both the number of infected sites and the coinfection frequency were calculated on the basis of observations at 48 hpi. Means ± standard deviations of three replicated leaves are shown.
[e] RNA1 + RNA2.NLS-YFP.p19 + RNA2.NLS-CFP.p19.

Numerical analysis of spatial separation of the two fluorescent protein vectors. Because an NLS was added to the fluorescent proteins, we could observe the strong nuclear fluorescence and carry out numerical analysis of the infected cells accurately using infected *C. quinoa* leaf samples. To describe the spatial separation of the two fluorescent protein vectors corresponding to the development of the infected regions, we defined three classes of the cells by their distance from the initially infected cells: initially infected cells (Cell-0), adjacent cells (Cell-1), and following cells (Cell-2) (Fig. 4A). However, as it is difficult to tell which cell is Cell-0, Cell-1, or Cell-2 in actual observations, raw data were first collected as mixtures of two or three classes of cells, and after the data from each infected

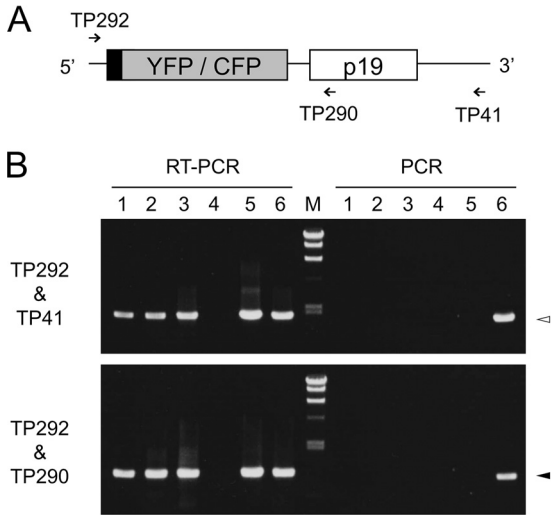

FIG. 3. RT-PCR and PCR amplifications of RNA2 vector and control templates. (A) Primers used for RT-PCR and PCR amplification. (B) RT-PCR (left halves) and PCR (right halves) products of RNA or DNA templates using primer sets TP292 and TP41 (upper panel) and TP292 and TP290 (lower panel). Templates (lanes): 1, total RNA isolated at 28 hpi; 2, total RNA isolated at 48 hpi; 3, total RNA isolated at 72 hpi; 4, total RNA isolated from healthy plant; 5, inoculated RNA transcript; 6, template DNA used for transcription. M, λDNA/HindIII marker with 23.1, 9.4, 6.6, 4.4, 2.3, and 2.0 kbp from the top. Arrowheads indicate the expected RT-PCR or PCR product sizes, 1,854 bp (upper panel, white arrowhead) and 1,070 bp (lower panel, black arrowhead).

TABLE 3. Mutations detected after cloning of RT-PCR or PCR product of infecting RNA2 vector and control templates

RT-PCR or PCR template	No. of clones with result/total no. of clones				Frequency of point mutation[d]
	Without nucleotide change	Without amino acid change	With deletion mutation	With point mutation(s)[c]	
Total RNA at 72 hpi[a]	14/23	16/23	2/23	7/23 (5/23)	8/16,422
Inoculated RNA transcript[a]	14/22	17/22	0/22	8/22 (5/22)	11/15,708
Template cDNA used for transcription[b]	10/24	14/24	0/24	14/24 (10/24)	24/17,136

[a] RT-PCR product of total RNA at 72 hpi or inoculated RNA transcript.
[b] PCR product of template DNA used for transcription.
[c] Numbers of clones with nucleotide substitution(s) or single-nucleotide insertion(s) are shown. Numbers in parentheses show clones with amino acid changes.
[d] Number of total point mutations/total number of sequenced nucleotides.

site were summed up, total cell numbers were divided into the classes by simple calculation (Table 1). Detailed calculation procedures were as follows (for schematic explanation, see Fig. S1 in the supplemental material). We assumed that the number of cells classified as Cell-1 is 8 per infected site from our observation. At 22 hpi, most of the infected sites showed 5 to 9 fluorescent cells, and these 158 sites with coinfection were regarded as Cell-0+Cell-1. The number of Cell-0 cells equals the number of the infected sites, and all the Cell-0 cells should be coinfected cells. Thus, the infection status of Cell-1 cells was estimated by subtracting the number of sites (i.e., 158) from the number of YFP+CFP cells (i.e., 945), resulting in 77 YFP-only cells, 787 YFP+CFP cells, and 82 CFP-only cells. Similarly, at 28 hpi, most of the infected sites showed 10 to 30 infected cells, and these 86 sites with coinfection were regarded as Cell-0+Cell-1+Cell-2. Cell-2 infection status was estimated by subtracting the number of the sites (i.e., 86) of Cell-0 cells from the YFP+CFP number (i.e., 1,163) and subtracting the number of the sites $\times$ 8 (i.e., 86 $\times$ 8 = 688) of Cell-1 cells from the YFP-only, YFP+CFP, or CFP-only numbers at the proportion calculated from the Cell-1 calculation result [i.e., (77 + 82)/2:787:(77 + 82)/2 = 0.084:0.832:0.084], respectively. Our calculation showed that starting from coinfected Cell-0 cells, 83.2% of Cell-1 and 61.6% of Cell-2 cells continuously showed coinfection, and others showed exclusive infection by only one of the two vector viruses (Table 1).

Model and idea for estimating of the size of genetic bottlenecks. We speculated that the spatial separation occurs because only limited numbers of virus vector genomes can establish infection in newly infected cells, and this limitation should be working as a genetic bottleneck for the intracellular populations. In order to estimate the number of founder viral genomes to establish infection in adjacent cells (i.e., the size of bottlenecks), we built a model as follows. First, settlement of founder genomes was regarded as a stochastic event described by the binominal distribution between two alleles, YFP and CFP: when k genomes are extracted from the mixture of YFP and CFP vectors mixed at the ratio of r:(1$-r$), occupation of extracted k genomes by YFP vectors (i.e., exclusive infection by YFP vector) will be observed at the probability of r^k, occupation by CFP vectors (i.e., exclusive infection by CFP vector) at $(1-r)^k$, and mixed genomes (i.e., coinfection) at $1-r^k-(1-r)^k$ (Fig. 4B). The fundamental idea was to find the most likely value for k by comparing this expected ratio with the observed ratio of exclusive infection to coinfection using the maximum-likelihood method. Second, variations in the size of bottleneck k were described by the Poisson distribution, with the mean λ_0, λ_1 and λ_2, respectively, for establishment of infection in Cell-0, Cell-1, and Cell-2 cells (Fig. 4C). Third, we assumed that infection of a single cell occurs by founder genomes from an adjacent single infected cell, not from multiple cells.

Estimation of the size of genetic bottlenecks. By the above model, the overall probability of coinfected sites (i.e., coinfected initial cells: Cell-0) [$P_{mix(site)}$] was described by two parameters: r_0, the ratio of YFP vector in inocula, and λ_0, the mean size of the bottleneck in initial cell infection, as follows:

$$P_{mix(site)} = p_0 \cdot 0 + p_1 \cdot 0 + \sum_{k_0=2}^{\infty} p_{k_0} \cdot \left[1 - r_0^{k_0} - (1-r_0)^{k_0}\right]$$

$$= \sum_{k_0=1}^{\infty} \left[1 - r_0^{k_0} - (1-r_0)^{k_0}\right] \frac{\lambda_0^{k_0}}{k_0!} e^{-\lambda_0}$$

$$= e^{-\lambda_0}\left[e^{\lambda_0} - 1 - (e^{\lambda_0 r_0} - 1) - (e^{\lambda_0(1-r_0)} - 1)\right]$$

$$= 1 + e^{-\lambda_0} - e^{(r_0-1)\lambda_0} - e^{-r_0\lambda_0}$$

where the probability of establishment of infection by k genomes (p_k) was described by Poisson distribution as $p_k = \frac{\lambda_0^k}{k!} e^{-\lambda_0}$. Note that $k_0 = 1$ was included in the summation in the second line because this makes the result in the square brackets zero. The likelihood of the numbers of coinfected sites (i.e., 179) and exclusively infected sites (i.e., 24) by one of the two vectors was described by the binomial distribution

$$L_0 = {}_{203}C_{179} \cdot P_{mix(site)}{}^{179}(1 - P_{mix(site)})^{24}$$

The likelihood of coinfection of adjacent cells (Cell-1 cells) is a little more complicated, because infection of Cell-1 cells is affected by the proportion of YFP and CFP vectors in each

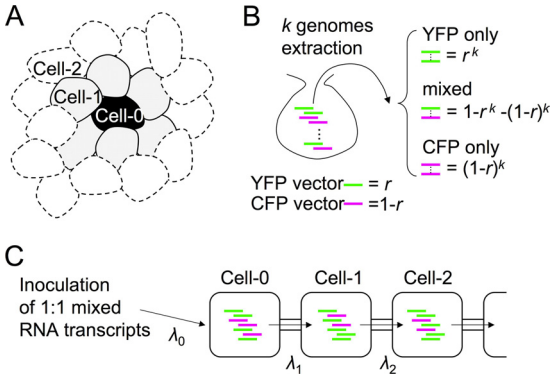

FIG. 4. Fundamental ideas and definitions in this work. (A) Schematic representation of classification of cells by distance from initially infected cell. (B) Settlement of founder genomes was regarded as stochastic event described by a binominal distribution between two alleles, YFP and CFP. (C) Average numbers of genomes to establish infection in Cell-0, Cell-1, and Cell-2 were defined as λ_0, λ_1, and λ_2, respectively.

Cell-0 [i.e., r_1: $(1-r_1)$]. Defining the number of founder YFP vectors that established infections in Cell-0 as l_0 and the mean size of the bottleneck for adjacent cell infection as λ_1, and assuming that final proportion of YFP and CFP vectors in Cell-0 follows the initial ratio of founder YFP and CFP vector [i.e., r_1: $(1-r_1)$ = l_0: (k_0-l_0)], the overall probability of coinfection of Cell-1 [$P_{mix(Cell\text{-}1)}$] in coinfected sites was described as follows:

$$P_{mix(Cell-1)} = \sum_{k_0=1}^{\infty}\sum_{l_0=1}^{k_0-1}\sum_{k_1=1}^{\infty} p^{(1)}_{k_0 l_0}\cdot\left[1-{r_1}^{k_1}-(1-r_1)^{k_1}\right]\cdot\frac{{\lambda_1}^{k_1}}{k_1!}e^{-\lambda_1}$$

$$= \sum_{k_0=1}^{\infty}\sum_{l_0=0}^{k_0}\sum_{k_1=1}^{\infty} p^{(1)}_{k_0 l_0}\cdot\left[1-\left(\frac{l_0}{k_0}\right)^{k_1} - \left(1-\frac{l_0}{k_0}\right)^{k_1}\right]\cdot\frac{{\lambda_1}^{k_1}}{k_1!}e^{-\lambda_1}$$

$$= \sum_{k_0=1}^{\infty}\sum_{l_0=0}^{k_0} p^{(1)}_{k_0 l_0}\cdot e^{-\lambda_1}\left[e^{\lambda_1}-1-\left(e^{\lambda_1\frac{l_0}{k_0}}-1\right) - \left(e^{\lambda_1\left(1-\frac{l_0}{k_0}\right)}-1\right)\right]$$

where $p^{(1)}_{k_0 l_0} = \frac{1}{P_{mix(site)}}\cdot\frac{{\lambda_0}^{k_0}}{k_0!}e^{-\lambda_0}\cdot{}_{k_0}C_{l_0}\cdot{r_0}^{l_0}(1-r_0)^{k_0-l_0}$. Noting the binomial formula, it was further simplified as

$$P_{mix(Cell-1)} = \sum_{k_0=1}^{\infty}\frac{1}{P_{mix(site)}}\cdot\frac{{\lambda_0}^{k_0}}{k_0!}e^{-\lambda_0}\cdot e^{-\lambda_1}\left[e^{\lambda_1}+1 - \left(r_0 e^{\frac{\lambda_1}{k_0}}+1-r_0\right)^{k_0} - \left(r_0+e^{\frac{\lambda_1}{k_0}}(1-r_0)\right)^{k_0}\right]$$

$$= \sum_{k_0=1}^{\infty}\frac{1}{P_{mix(site)}}\cdot\frac{{\lambda_0}^{k_0}}{k_0!}e^{-\lambda_0}\cdot\left[1+e^{-\lambda_1} - \left(r_0+e^{-\frac{\lambda_1}{k_0}}(1-r_0)\right)^{k_0} - \left(r_0 e^{-\frac{\lambda_1}{k_0}}+1-r_0\right)^{k_0}\right]$$

The likelihood of the estimated number of coinfected Cell-1 cells (i.e., 787) and the estimated number of exclusively infected Cell-1 cells by one of the two vectors (i.e., 159) was described as

$$L_1 = {}_{946}C_{787}\cdot {P_{mix(Cell-1)}}^{787}(1-P_{mix(Cell-1)})^{159}.$$

Similarly, defining the mean size of the bottleneck for following-cell infection as λ_2, the overall probability of coinfection of the following cells (i.e., Cell-2) in coinfected sites [$P_{mix(Cell\text{-}2)}$] was described as follows:

$$P_{mix(Cell-2)} = \sum_{k_1=1}^{\infty}\sum_{l_1=0}^{k_1} p^{(2)}_{k_1 l_1}\cdot e^{-\lambda_2}\left[e^{\lambda_2}-1-\left(e^{\lambda_2\frac{l_1}{k_1}}-1\right) - \left(e^{\lambda_2\left(1-\frac{l_1}{k_1}\right)}-1\right)\right]$$

where

$$p^{(2)}_{k_1 l_1} = \frac{1}{P_{mix(site)}}\cdot\sum_{k_0=1}^{\infty}\sum_{l_0=1}^{k_0-1}\frac{{\lambda_0}^{k_0}}{k_0!}e^{-\lambda_0}\cdot{}_{k_0}C_{l_0} \cdot {r_0}^{l_0}(1-r_0)^{k_0-l_0}\cdot\frac{{\lambda_1}^{k_1}}{k_1!}e^{-\lambda_1}\cdot{}_{k_1}C_{l_1}\cdot{r_1}^{l_1}(1-r_1)^{k_1-l_1}$$

$$= \frac{1}{P_{mix(site)}}\cdot\sum_{k_0=1}^{\infty}\sum_{l_0=0}^{k_0}\frac{{\lambda_0}^{k_0}}{k_0!}e^{-\lambda_0}\cdot{}_{k_0}C_{l_0} \cdot {r_0}^{l_0}(1-r_0)^{k_0-l_0}\cdot\frac{{\lambda_1}^{k_1}}{k_1!}e^{-\lambda_1}\cdot{}_{k_1}C_{l_1}\cdot\left(\frac{l_0}{k_0}\right)^{l_1}\left(1-\frac{l_0}{k_0}\right)^{k_1-l_1}$$

Using the binomial formula, $P_{mix(Cell\text{-}2)}$ was reduced to

$$P_{mix(Cell-2)} = \frac{1}{P_{mix(site)}}\cdot\sum_{k_1=1}^{\infty}\frac{{\lambda_1}^{k_1}}{k_1!}e^{-\lambda_1}\cdot\sum_{k_0=1}^{\infty}\frac{{\lambda_0}^{k_0}}{k_0!}e^{-\lambda_0}\cdot\sum_{l_0=0}^{k_0}{}_{k_0}C_{l_0} \cdot {r_0}^{l_0}(1-r_0)^{k_0-l_0}\left[1+e^{-\lambda_2} - \left(\frac{l_0}{k_0}+e^{-\frac{\lambda_2}{k_1}}\left(1-\frac{l_0}{k_0}\right)\right)^{k_1} - \left(\frac{l_0}{k_0}e^{-\frac{\lambda_2}{k_1}}+1-\frac{l_0}{k_0}\right)^{k_1}\right]$$

and the likelihood was described as

$$L_2 = {}_{819}C_{505}\cdot {P_{mix(Cell-2)}}^{505}(1-P_{mix(Cell-2)})^{314}$$

based on the estimated number of coinfected Cell-2 cells and the estimated number of Cell-2 cells exclusively infected by one of the two vectors.

Then, substituting 0.5 for r_0, we simultaneously estimated λ_0, λ_1, and λ_2 by maximizing the total log likelihood

$$\log L = \log L_0 + \log L_1 + \log L_2$$

Calculation was done using statistical computing software R (22), and we obtained the mean bottleneck sizes $\lambda_0 = 5.59 \pm 0.40$, $\lambda_1 = 5.97 \pm 0.22$, and $\lambda_2 = 5.02 \pm 0.29$ (maximum likelihood estimates ± standard errors).

These results indicate that only around 5 to 6 founder genomes establish infection in adjacent cells after cell-to-cell movement. The expected size of bottlenecks for the second cell-to-cell movement (λ_2) was slightly smaller than that for first cell-to-cell movement (λ_1).

Evaluation of the model and the estimated bottleneck sizes by comparing simulation and observation results. The estimated bottleneck sizes were used to simulate the decrease in coinfected cells corresponding to the development of infected regions. Assuming that the mean number of viral genomes that establish infection in Cell-N (λ_N, $N \geq 3$) equals λ_2, the overall probability of coinfected cells in Cell-N [$P_{mix(Cell\text{-}N)}$, $N \geq 3$] in coinfected sites was simulated by recurrence relation as follows:

$$P_{mix(Cell-N)} = \sum_{k_{N-1}=1}^{\infty}\sum_{l_{N-1}=0}^{k_{N-1}} p^{(N)}_{k_{N-1} l_{N-1}}\cdot e^{-\lambda_2}\left[e^{\lambda_2}-1-\left(e^{\lambda_2\frac{l_{N-1}}{k_{N-1}}}-1\right) - \left(e^{\lambda_2\left(1-\frac{l_{N-1}}{k_{N-1}}\right)}-1\right)\right]$$

where

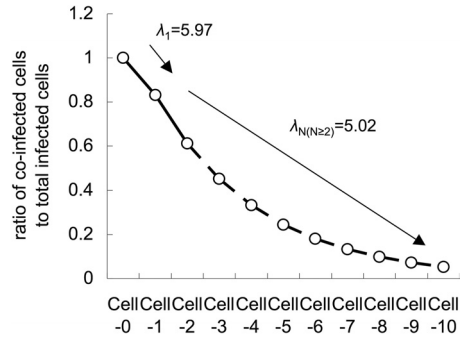

FIG. 5. Simulation of the decrease of coinfected cells corresponding to the development of locally infected regions. The dashed line represents simulated results, while the solid line represents observed results.

$$p^{(N)}_{k_{N-1}l_{N-1}} = \sum_{k_{N-2}=1}^{\infty} \sum_{l_{N-2}=0}^{k_{N-2}} p^{(N-1)}_{k_{N-2}l_{N-2}} \cdot \frac{\lambda_2^{k_{N-1}}}{k_{N-1}!} e^{-\lambda_2} \cdot {}_{k_{N-1}}C_{l_{N-1}} \cdot \left(\frac{l_{N-2}}{k_{N-2}}\right)^{l_{N-1}} \cdot \left(1 - \frac{l_{N-2}}{k_{N-2}}\right)^{k_{N-1} - l_{N-1}}$$

and

$$p^{(2)}_{k_1 l_1} = \frac{1}{P_{mix(site)}} \cdot \sum_{k_0=1}^{\infty} \sum_{l_0=0}^{k_0} \frac{\lambda_0^{k_0}}{k_0!} e^{-\lambda_0} \cdot {}_{k_0}C_{l_0} \cdot r_0^{l_0}(1 - r_0)^{k_0 - l_0} \cdot \frac{\lambda_1^{k_1}}{k_1!} e^{-\lambda_1} \cdot {}_{k_1}C_{l_1} \cdot \left(\frac{l_0}{k_0}\right)^{l_1} \left(1 - \frac{l_0}{k_0}\right)^{k_1 - l_1}$$

where $P_{mix(site)} = 179/203$, $r_0 = 0.5$, $\lambda_0 = 5.59$, $\lambda_1 = 5.97$, and $\lambda_2 = 5.02$. The simulation result showed that fewer than 10% of coinfected cells would be observed in Cell-8 cells (Fig. 5). This simulation result is consistent with our actual observations at 72 hpi, when most of the infected sites show absolute spatial separation by 7 to 9 cell-to-cell movements (Fig. 2D), indicating that our model and the estimated sizes of the bottlenecks are reliable.

Simulation of enhanced selection on *trans*-acting elements caused by narrow genetic bottlenecks. As we observed, rapid spatial separation occurs between two artificial vector genomes during the development of locally infected regions by a plant virus. This phenomenon can be explained by the idea that rapid fixation of an allele occurs in bottlenecked populations (15). We extended this idea to model the rapid selection of *trans*-acting genes or elements in plant RNA viral genomes.

Some of the sources of genetic information in RNA viral genomes, such as 5′ and 3′ untranslated regions (UTRs), work in *cis* to the viral genomes, while others, such as MP and p19 of SBWMV expressed from subgenomic RNAs, work in *trans*. These *trans*-acting elements or gene products should be shared among intracellular populations of viral genomes. Thus, the selection of *trans*-acting genes or elements should be slow compared to the selection of *cis*-acting genes or elements because of complementation by adaptive genomes for defective ones in intracellular populations. We speculated that narrow genetic bottlenecks would solve this problem by stochastically isolating adaptive genomes from defective genomes, allowing adaptive genomes to benefit exclusively from the mutations in their genomes (Fig. 6A). Therefore, we investigated how bottleneck sizes affect the speed of selection on *trans*-acting genes or elements by modeling the competition between intracellular populations, among which narrow bottlenecks create variety in the ratios of adaptive genomes to defective genomes.

Competition between intracellular populations was modeled by different probabilities of establishment of infection in adjacent cells: the probabilities of succession of intracellular populations (S). S was described by logistic curve with respect to the proportion of adaptive genomes in the intracellular population $\left(\frac{A}{N_e}\right)$

$$S^{\frac{A}{N_e}} = \frac{1}{1 + e^{c\left(a_0 - \frac{A}{N_e}\right)}}$$

Here N_e (effective population number) is the size of the bottleneck (i.e., the number of viral genomes that establish infection, MOI) and A is the number of adaptive genomes in total N_e genomes. We assumed $a_0 = 0.3$ and $c = 30$; a_0 and c determine the inflection point and inclination of the logistic curve, respectively. We used $a_0 = 0.3$ because an SBWMV RNA2 mutant with ~30% transcription efficiency of p19 subgenomic RNA compared to that of wild-type virus could infect plants but showed irregular formed lesions (34), indicating that the virus can infect some cells but not others. With these parameter values, the succession probability of intracellular probability is very low if the frequency of the adaptive genome is below 0.2, while it is close to 1 if the frequency is over 0.4 (Fig. 6B).

The ratio of cells infected by A adaptive genome and $N_e - A$ defective genomes in Cell-N ($r_{(Cell-N)N_eA_N}$) was described as follows:

$$r_{(Cell-N)N_eA_N} = \frac{\sum_{A_{N-1}=0}^{N_e} S^{\frac{A_{N-1}}{N_e}} \cdot r_{(Cell-N-1)N_eA_{N-1}} \cdot {}_{N_e}C_{A_{N-1}} \cdot \left(\frac{A_{N-1}}{N_e}\right)^{A_N} \left(1 - \frac{A_{N-1}}{N_e}\right)^{N_e - A_N}}{\sum_{A_{N-1}=0}^{N_e} S^{\frac{A_{N-1}}{N_e}} \cdot r_{(Cell-N-1)N_eA_{N-1}}}.$$

Assuming that there are abundant cells to receive intracellular populations, the ratio of adaptive genomes to the total population of Cell-N cells ($R_{(Cell-N)N_e}$) was described as follows:

$$R_{(Cell-N)N_e} = \sum_{A_N=0}^{N_e} \frac{A_N}{N_e} \cdot r_{(Cell-N)N_eA_N}$$

Using the above model, exclusion of defective mutant genomes was tested. Starting from a mixed virus population with 80% adaptive genomes and 20% defective genomes (i.e., $r_{(Cell-1)N_eA_1} = 0.8$), rapid exclusion of the defective genome was observed for smaller N_e values (e.g., 5 or 10), while almost no change was observed for larger N_e values (e.g., 50 or 100) in 10 cell-to-cell movements (Fig. 6C). Similarly, selection of an adaptive mutation was tested. Starting from a mixed virus population with 20% adaptive genomes and 80% defective

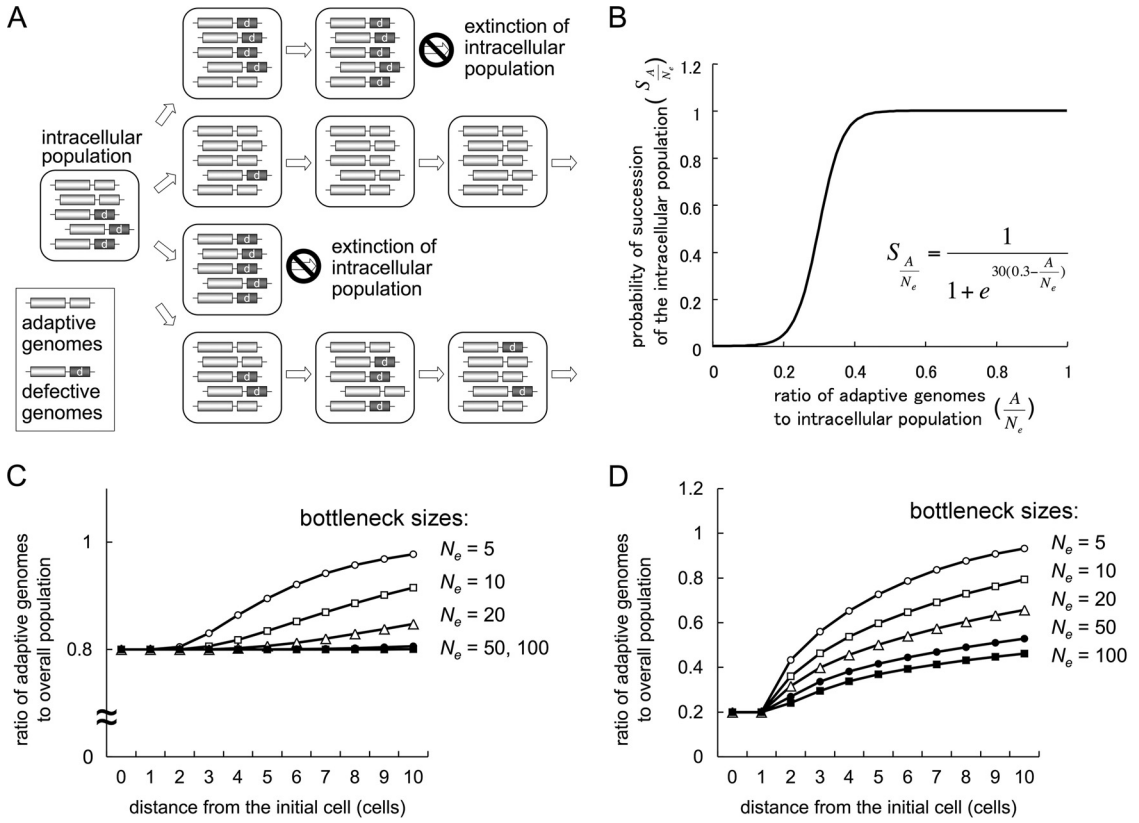

FIG. 6. Idea and simulation results of effective selection on *trans*-acting elements due to narrow genetic bottlenecks. (A) Schematic representation of a mechanism for effective selection on *trans*-acting elements. Narrow genetic bottlenecks in cell-to-cell movements stochastically isolate adaptive genomes from defective genomes, resulting in rapid selection for adaptive genomes. (B) Modeling of competition among intracellular populations by describing their probabilities of succession (S) with respect to the proportion of adaptive genomes in the intracellular population $\left(\frac{A}{N_e}\right)$. (C) Simulation of the exclusion of defective genomes with different bottleneck sizes (N_e). Note that initial ratios of adaptive and defective genomes are 80% and 20%, respectively. (D) Simulation of the selection of adaptive genomes with different bottleneck sizes (N_e). Initial ratios of adaptive and defective genomes are 20% and 80%, respectively.

genomes (i.e., $r_{(Cell-1)N_eA_1} = 0.2$), rapid occupation by the adaptive genome was observed for smaller N_e values (e.g., 5 or 10), while a slower change was observed for larger N_e values (e.g., 50 or 100) (Fig. 6D). On the other hand, a similar simulation modeling selection of *cis*-acting elements between adaptive genomes and less-adaptive genomes with 1:0.5 replication efficiencies showed that selection would rapidly occur almost independently of the size of bottlenecks (data not shown). We also confirmed that the simulation results are not largely affected by changing a_0 and c (data not shown).

DISCUSSION

By observing the spatial separation of virus vectors carrying two different fluorescent proteins, we have shown that narrow genetic bottlenecks occur during cell-to-cell movement of a plant RNA virus in the leaves of the natural host and local lesion host. The estimated size of bottlenecks was surprisingly small, with averages of 5.97 ± 0.22 for first cell-to-cell movement and 5.02 ± 0.29 for second cell-to-cell movement. The underestimation effect of deletion mutations in fluorescent protein coding regions should be around 3 to 4% at the time points we carried out estimations (i.e., 22 and 28 hpi), because only fewer than 10% of deletion mutants were observed at 72 hpi. The estimated sizes of the bottlenecks are similar to those in the recent report by Gonzalez-Jara et al. (10), which showed that the MOI in plant tissue colonization (i.e., the size of bottlenecks) decreases from 6 to 1 to 2, corresponding to the expansion of the TMV-infected regions. The similarity of their and our estimated sizes indicates that narrow genetic bottlenecks in cell-to-cell movements are generally occurring with plant RNA viruses that infect mesophyll cells. However, we consider it difficult to say that decreases in the size of bottlenecks are generally occurring phenomena, because the estimations are affected by how we model the plant tissues. For example, we carried out our estimation assuming that the number of Cell-1 cells per an infected Cell-0 cell is eight and obtained $\lambda_1 = 5.97 \pm 0.22$ and $\lambda_2 = 5.02 \pm 0.29$; however, if we assumed the number is six or seven, we would obtain $\lambda_1 = 5.86 \pm 0.29$ and $\lambda_2 = 5.72 \pm 0.38$ or $\lambda_1 = 6.02 \pm 0.25$ and $\lambda_2 = 5.19 \pm 0.30$, respectively, indicating that there are negative relationships between the estimated sizes of the latter bottleneck and the assumed ratios of newly infected cells to source cells. Gonzalez-Jara et al. (10) carried out their estimations assuming that the ratio is always 6.5, but according to our

understanding, as this ratio will rapidly decrease to almost 1 corresponding to the expansion of the infected regions (for two models to suggest the decrease in the ratio, see Fig. S2 in the supplemental material), they may have underestimated the sizes of bottlenecks at later time points. Accumulation of deletion mutations may also cause an underestimation of the sizes of bottlenecks at later time points. On the other hand, our model may slightly overestimate the sizes of bottlenecks because of the simplification that infection of a single cell occurs by founder genomes from an adjacent single infected cell. Thus, the changes in the sizes of bottlenecks during host colonization should be discussed further, especially with more attention paid to the way to model plant tissues, accumulation of deletion mutants, and spread of virus infection.

We do not know the mechanisms of the occurrence of the bottlenecks during cell-to-cell movement. However, we speculate that the bottleneck may not be a physical matter in cell-to-cell movement, because the number of plasmodesmata connecting two mesophyll cells is estimated to be 26, on average, using spinach leaves (31), which belong to the same family with *C. quinoa*, Chenopodiaceae, indicating that there are enough plasmodesmata for the virus to go through. Studies of replication complexes of hepatitis C virus (HCV) (32) and virus-induced mini-organelles, in which viral replication occur, of Flock House virus (FHV) (16) have shown that several hundred replication complexes and around 11 thousand virus-induced mini-organelles are formed when the viruses infect a host cell. Comparing the estimated bottleneck sizes with these results, it is reasonable to consider that the bottleneck event (i.e., the settlement of the founder virus) occurs prior to the formation of replication complexes or virus-induced mini-organelles. From this viewpoint, competition for resources required for genome replication or protein expression can be also excluded from the mechanisms of the bottleneck, because the bottleneck events seem to occur before the viral replication and protein expression become vigorous. As demonstrated by previous research on WSMV bottlenecks in systemic movement (11), bottlenecks during cell-to-cell movement may also occur due to sequence homology, probably via an RNA silencing mechanism to refuse additional infection by a virus with sequence homology. This idea can explain the fact that SBWMV does not suffer from narrow genetic bottlenecks in spite of its bipartite genome, because only a limited bottleneck effect between RNA1 and RNA2 will be expected. Further studies of the mechanisms and the timing of the occurrence of genetic bottlenecks are required.

Previous research on bacteriophage (4, 6) and animal (7, 8, 36) and plant (5) RNA viruses showed that repeated bottleneck events, caused by transferring plaques or lesions, resulted in fitness losses for viral genomes because of the mechanism known as Muller's ratchet (21). Our observations and estimations showed that intracellular populations of a plant virus face narrow genetic bottlenecks in every cell-to-cell movement, and, following this idea, bottlenecks should cause extinction or very low mean fitness of the populations. This may be the case for the history of an intracellular population traveling from one cell to another cell. However, because there are abundant cells and spaces for local infection in a host plant to receive viral intracellular populations, stochastically adaptive genomes persist or appear, and survival of the viral population as a whole will be achieved. Why have plant viruses not evolved to avoid bottlenecks? We speculate that the plant viruses are actually utilizing the bottlenecks as an essential element of their evolution mechanisms. In this study, we focused on viral elements working in *trans* to their genomes, which would not receive selection pressure as effectively as *cis*-acting elements because of the complementation in intracellular populations. Simulating this situation by describing competition among intracellular populations, our model implied that narrow genetic bottlenecks during cell-to-cell movement help the selection pressure to work on *trans*-acting genes or elements by rapidly isolating the adaptive genomes from defective genomes. This system may counteract the negative effect of bottlenecks (i.e., fitness losses), and, furthermore, it may enable the plant RNA virus to rapidly respond to changes such as temperature shift, condition changes in different organs of a host, host shifting and so on. Interestingly, a study of φ6, a lytic RNA bacteriophage, showed that repeated large population transfers with broadened bottlenecks result in occupation of the viral population by "selfish" genomes, each of which cannot effectively replicate by itself but can replicate well only among the intracellular population because of complementation (30). A similar situation could occur in plant RNA virus infection of a host plant if the bottleneck sizes in cell-to-cell movement were large, resulting in ineffective plant-to-plant transmission because of the bottlenecked transmission of selfish genomes, each of which cannot replicate well by itself. Thus, roughly constant but variable bottleneck sizes in cell infection through their life cycles (i.e., cell-to-cell movement, vascular to mesophyll cell invasion, and so on) may be favored for plant RNA virus evolution.

In conclusion, we demonstrated narrow genetic bottlenecks and their estimated sizes during cell-to-cell movement of a plant virus, and we created a simple model to explain why plant RNA viruses do not suffer from the bottlenecks. We believe this work provides a new insight into survival strategies and population dynamics of plant RNA viruses.

ACKNOWLEDGMENTS

We thank Yukio Shirako (ANESC, Univ. of Tokyo) for providing us with infectious cDNA constructs for SBWMV, pJS1 and pJS2, used in this study. We also thank anonymous reviewers for critical and constructive comments, which improved the manuscript significantly.

S.M. was supported by the Japan Society for the Promotion of Sciences (JSPS) Research Fellowships for Young Scientists (20-5665) and the Japan Science Technology Agency (JST) PRESTO program. H.K. was supported by a Grant-in-Aid for Scientific Research (B-19300094) from JSPS.

REFERENCES

1. **Ali, A., H. Li, W. L. Schneider, D. J. Sherman, S. Gray, D. Smith, and M. J. Roossinck.** 2006. Analysis of genetic bottlenecks during horizontal transmission of cucumber mosaic virus. J. Virol. **80:**8345–8350.
2. **An, H., U. Melcher, P. Doss, M. Payton, A. C. Guenzi, and J. Verchot-Lubicz.** 2003. Evidence that the 37 kDa protein of soil-borne wheat mosaic virus is a virus movement protein. J. Gen. Virol. **84:**3153–3163.
3. **Betancourt, M., A. Fereres, A. Fraile, and F. Garcia-Arenal.** 2008. Estimation of the effective number of founders that initiate an infection after aphid transmission of a multipartite plant virus. J. Virol. **82:**12416–12421.
4. **Chao, L.** 1990. Fitness of RNA virus decreased by Muller's ratchet. Nature **348:**454–455.
5. **de la Iglesia, F., and S. F. Elena.** 2007. Fitness declines in tobacco etch virus upon serial bottleneck transfers. J. Virol. **81:**4941–4947.
6. **de la Pena, M., S. F. Elena, and A. Moya.** 2000. Effect of deleterious mutation-accumulation on the fitness of RNA bacteriophage MS2. Evolution **54:**686–691.
7. **Duarte, E., D. Clarke, A. Moya, E. Domingo, and J. Holland.** 1992. Rapid

fitness losses in mammalian RNA virus clones due to Muller's ratchet. Proc. Natl. Acad. Sci. U. S. A. **89:**6015–6019.
8. **Escarmis, C., M. Davila, N. Charpentier, A. Bracho, A. Moya, and E. Domingo.** 1996. Genetic lesions associated with Muller's ratchet in an RNA virus. J. Mol. Biol. **264:**255–267.
9. **French, R., and D. C. Stenger.** 2003. Evolution of wheat streak mosaic virus: dynamics of population growth within plants may explain limited variation. Annu. Rev. Phytopathol. **41:**199–214.
10. **Gonzalez-Jara, P., A. Fraile, T. Canto, and F. Garcia-Arenal.** 2009. The multiplicity of infection of a plant virus varies during colonization of its eukaryotic host. J. Virol. **83:**7487–7494.
11. **Hall, J. S., R. French, G. L. Hein, T. J. Morris, and D. C. Stenger.** 2001. Three distinct mechanisms facilitate genetic isolation of sympatric wheat streak mosaic virus lineages. Virology **282:**230–236.
12. **Ishikawa, M., T. Meshi, F. Motoyoshi, N. Takamatsu, and Y. Okada.** 1986. In vitro mutagenesis of the putative replicase genes of tobacco mosaic virus. Nucleic Acids Res. **14:**8291–8305.
13. **James, P., J. Halladay, and E. A. Craig.** 1996. Genomic libraries and a host strain designed for highly efficient two-hybrid selection in yeast. Genetics **144:**1425–1436.
14. **Kawakami, S., K. Hori, D. Hosokawa, Y. Okada, and Y. Watanabe.** 2003. Defective tobamovirus movement protein lacking wild-type phosphorylation sites can be complemented by substitutions found in revertants. J. Virol. **77:**1452–1461.
15. **Kimura, M., and T. Ohta.** 1969. The average number of generations until fixation of a mutant gene in a finite population. Genetics **61:**763–771.
16. **Kopek, B. G., G. Perkins, D. J. Miller, M. H. Ellisman, and P. Ahlquist.** 2007. Three-dimensional analysis of a viral RNA replication complex reveals a virus-induced mini-organelle. PLoS Biol. **5:**e220.
17. **Kremers, G. J., J. Goedhart, E. B. van Munster, and T. W. Gadella, Jr.** 2006. Cyan and yellow super fluorescent proteins with improved brightness, protein folding, and FRET Forster radius. Biochemistry **45:**6570–6580.
18. **Li, H., and M. J. Roossinck.** 2004. Genetic bottlenecks reduce population variation in an experimental RNA virus population. J. Virol. **78:**10582–10587.
19. **Malpica, J. M., A. Fraile, I. Moreno, C. I. Obies, J. W. Drake, and F. Garcia-Arenal.** 2002. The rate and character of spontaneous mutation in an RNA virus. Genetics **162:**1505–1511.
20. **Moury, B., F. Fabre, and R. Senoussi.** 2007. Estimation of the number of virus particles transmitted by an insect vector. Proc. Natl. Acad. Sci. U. S. A. **104:**17891–17896.
21. **Muller, H. J.** 1964. The relation of recombination to mutational advance. Mutat. Res. **106:**2–9.
22. **R Development Core Team.** 2005. R: a language and environment for statistical computing. R Foundation for Statistical Computing, Vienna, Austria. http://www.R-project.org.
23. **Roossinck, M. J., and W. L. Schneider.** 2006. Mutant clouds and occupation of sequence space in plant RNA viruses. Curr. Top. Microbiol. Immunol. **299:**337–348.
24. **Sacristan, S., J. M. Malpica, A. Fraile, and F. Garcia-Arenal.** 2003. Estimation of population bottlenecks during systemic movement of tobacco mosaic virus in tobacco plants. J. Virol. **77:**9906–9911.
25. **Shirako, Y.** 1998. Non-AUG translation initiation in a plant RNA virus: a forty-amino-acid extension is added to the N terminus of the soil-borne wheat mosaic virus capsid protein. J. Virol. **72:**1677–1682.
26. **Shirako, Y., and M. K. Brakke.** 1984. Spontaneous deletion mutation of soil-borne wheat mosaic virus RNA II. J. Gen. Virol. **65:**855–858.
27. **Shirako, Y., and M. K. Brakke.** 1984. Two purified RNAs of soil-borne wheat mosaic virus are needed for infection. J. Gen. Virol. **65:**119–127.
28. **Shirako, Y., and T. M. Wilson.** 1993. Complete nucleotide sequence and organization of the bipartite RNA genome of soil-borne wheat mosaic virus. Virology **195:**16–32.
29. **Te, J., U. Melcher, A. Howard, and J. Verchot-Lubicz.** 2005. Soilborne wheat mosaic virus (SBWMV) 19K protein belongs to a class of cysteine rich proteins that suppress RNA silencing. Virol. J. **2:**18.
30. **Turner, P. E., and L. Chao.** 1998. Sex and the evolution of intrahost competition in RNA virus phi6. Genetics **150:**523–532.
31. **Warmbrodt, R. D., and W. J. VanDerWoude.** 1990. Leaf of Spinacia oleracea (spinach): ultrastructure, and plasmodesmatal distribution and frequency, in relation to sieve-tube loading. Am. J. Bot. **77:**1361–1377.
32. **Wolk, B., B. Buchele, D. Moradpour, and C. M. Rice.** 2008. A dynamic view of hepatitis C virus replication complexes. J. Virol. **82:**10519–10531.
33. **Xin, H. W., and S. W. Ding.** 2003. Identification and molecular characterization of a naturally occurring RNA virus mutant defective in the initiation of host recovery. Virology **317:**253–262.
34. **Yamamiya, A., M. Miyanishi, and Y. Shirako.** 2005. Stable deletions arising in the readthrough region of soil-borne wheat mosaic virus RNA2 define the 5′ limit of the functional promoter for the p19 subgenomic RNA. Arch. Virol. **150:**1871–1884.
35. **Yamamiya, A., and Y. Shirako.** 2000. Construction of full-length cDNA clones to soil-borne wheat mosaic virus RNA1 and RNA2, from which infectious RNAs are transcribed In vitro: virion formation and systemic infection without expression of the N-terminal and C-terminal extensions to the capsid protein. Virology **277:**66–75.
36. **Yuste, E., S. Sanchez-Palomino, C. Casado, E. Domingo, and C. Lopez-Galindez.** 1999. Drastic fitness loss in human immunodeficiency virus type 1 upon serial bottleneck events. J. Virol. **73:**2745–2751.